Atom interferometer using spatially localized beam splitters

Clément Debavelaere,[1] Cyrille Solaro,[1] Saïda Guellati-Khélifa,[1,2] and Pierre Cladé[1]
[1]*Laboratoire Kastler Brossel, Sorbonne Université, CNRS, ENS-PSL, Collège de France, 4 place Jussieu, 75005 Paris, France*
[2]*Conservatoire National des Arts et Métiers, 292 rue Saint Martin, 75003 Paris, France*

(Received 17 April 2024; accepted 14 June 2024; published 12 July 2024)

A picosecond laser is used to realize atomic beam splitters based on stimulated Raman transitions. With this approach, the interaction between the laser and the atom is localized in the overlap zone of pairs of counterpropagating picosecond pulses. This imposes constraints for implementing interferometers on free-falling atoms. We have developed a robust technique to control the pulses' overlap and ensure that it follows the atom's trajectory while minimizing the induced laser phase noise. We also demonstrate an atom interferometer where the atomic beam splitters are applied to one arm of the interferometer without interacting with the atomic wave packet propagating along the other arm.

DOI: 10.1103/PhysRevA.110.013310

I. INTRODUCTION

To fully exploit the potential of atom interferometry and to extend its scope, a variety of new concepts and designs are currently being investigated and developed around the world. Current efforts aim at pushing to the extreme the sensitivity of atom interferometers for testing the fundamental laws of physics, for detecting gravitational waves in the low-frequency range [1–5], or searching for signatures of dark matter [6,7]. Work is also underway to develop compact and transportable inertial sensors based on atom interferometry for applications on the ground or in space [8]. All these experiments use continuous-wave (cw) laser sources to manipulate atomic wave packets. In 2022, we demonstrated that it is possible to implement coherent atomic beam splitters based on stimulated Raman transitions driven by two counterpropagating trains of picosecond laser pulses [9]. There are two main motivations to further explore this new technique. As for high-resolution spectroscopy, a first motivation for using a pulsed laser (or a frequency comb) rather than a cw laser is to extend light-pulse matter-wave interferometry to a broader spectral range and to more atomic species [10–15]. The second motivation relates to the fundamental difference between the use of a continuous wave and a pulsed laser. In the former case, laser-atom interaction takes place at the atoms' location, whereas in the latter it is determined by the overlap zone of pairs of counterpropagating ultrashort pulses. This specific feature is *a priori* a constraint that limits the interrogation time of free-falling atoms and therefore the interferometer's sensitivity. Yet, it offers the advantage of enabling atom interferometer configurations that are not feasible with a cw laser.

In this paper, we present a robust system we have implemented to dynamically and precisely control the position of the pulses' overlap zone during the interferometer sequence while compensating for the Doppler shift due to gravity. We did this using a controlled moving delay line, which would be equivalent to dropping the retroreflecting mirror. We achieved a maximum interrogation time of 50 ms, a fivefold increase compared with our previous work, limited by the range of a translation stage. We also demonstrate an original scheme of an atom interferometer where laser pulses interact selectively with atomic wave packets in either arm.

II. PHASE AND VELOCITY CONTROL

Our interferometer uses atomic beam splitters based on two-photon stimulated Raman transitions. To achieve this with a pulsed picosecond laser, each pulse is split in two, and a delay line is used to create two pulse trains that should overlap at the atom's position. The polarizations of the two pulses that induce the Raman transition are orthogonal (see our previous work [9]). The length of the delay line is set equal to the distance between the retroreflecting mirror and the initial position of the atomic cloud (see Fig. 1). An acousto-optic modulator (AOM-2) is inserted in the delay line. In our initial work, where the delay was fixed, this AOM was used to compensate for the Doppler shift by chirping the driving rf-frequency ν_{aom} according to

$$\nu_0 - \nu_{\mathrm{rec}} + k_{\mathrm{comb}}\alpha t = q f_{\mathrm{r}} + \nu_{\mathrm{aom}}(t). \tag{1}$$

In this equation, ν_0 is the frequency difference between the two hyperfine levels of the fundamental electronic state of ^{87}Rb, ν_{rec} is the recoil frequency, k_{comb} is twice the average wave vector of the picosecond laser, and f_{r} is the repetition rate of the picosecond laser. The integer q and repetition rate are chosen so that ν_{aom} matches with the frequency range of the AOM. To obtain the atomic fringes, we measure the population in the hyperfine levels $|F = 1\rangle$ and $|F = 2\rangle$ as a function of the frequency ramp α. In a vertical configuration, the position of the central fringe gives a direct measurement of the Earth's gravitational acceleration g.

To extend the interrogation time, in our new setup, we adjust the length of the delay line during the interferometer sequence. To do so, one mirror of the delay line is accelerated at a rate α ensuring that the overlap zone follows the free fall of the atomic cloud. The experimental setup and this mirror (M2) is shown in Fig. 1.

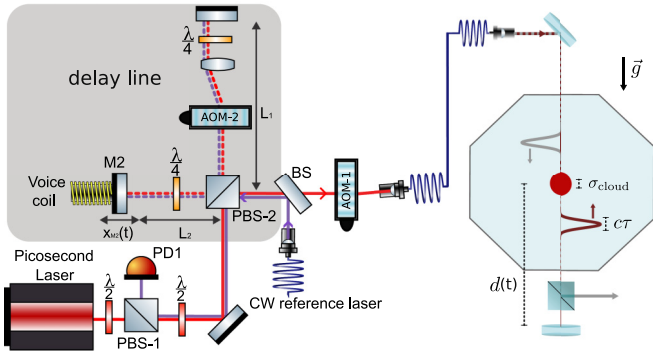

FIG. 1. Overview of our experimental setup. The picosecond laser (red line) is split in two on the polarizing beam splitter PBS-2. One part is sent directly to the vacuum chamber and is retroreflected by a mirror placed below the chamber. The other part passes through a delay line. The mirror M2 of the delay line is moved using a voice coil actuator. A cw reference laser, with a known wavelength (in purple), is used to measure the position of M2 using a heterodyne detection scheme.

We denote as $d(t)$ the distance between the bottom mirror and the atoms' position. The transmitted beam (red dashed line) enters the adjustable delay line $L_1 + L_2 + x_{M2(t)}$ before being coupled into the same optical fiber as the reflected beam. The mirror M2 is moved using a voice coil actuator (Thorlabs VC500/M) and its acceleration is controlled by driving a current into the coil. This both displaces the overlap position and chirps the frequency of the delayed beam. The mirror M2 must follow the free fall of the atoms $x_{ff}(t)$. This displacement not only allows us to follow the atomic cloud but it also naturally compensates for the Doppler effect. A cw laser (purple line Fig. 1) is used to measure the position of M2 using a heterodyne detection scheme. The beam splitter (BS) allows the cw beam to overlap with the trajectory of the pulsed beams, traveling in opposite directions. The displacement of M2 can then be deduced from the phase shift of the cw beatnote measured by the photodiode (PD1).

More precisely, the phase shift measured by the photodiode is given by

$$\Phi_{\text{beatnote}}(t) = 2\Phi_{\text{AOM}}(t) + k_{\text{CW}} x_{\text{M2}}(t), \tag{2}$$

where the factor 2 comes from the double pass configuration of the AOM.

To have a direct measurement of the error position $\Delta x(t) = x_{\text{ff}}(t) - x_{\text{M2}}(t)$, Φ_{beatnote} is demodulated with a signal

$$\Phi_{\text{demod}}(t) = 2\Phi_{\text{AOM}}(t) + k_{\text{CW}} x_{\text{ff}}(t) \tag{3}$$

giving

$$\Phi_{\text{error}}(t) = k_{\text{CW}} \Delta x(t). \tag{4}$$

The measurement of $\Phi_{\text{error}}(t)$ is used to retroact on the voice coil and adjust the mirror position.

To control both the acceleration of the mirror and the AOM, we use an FPGA (red pitaya board). Figure 2 describes the logic implemented. Two direct digital synthesizer (DDS) cores are implemented in the FPGA. The first DDS is used to control the AOM and the second to control the demodulation signal. Because the output frequency of the board is limited to 50 MHz, the signal is mixed with a constant frequency (ν_0) to shift the output to the 80 MHz range. The output of each DDS is defined by the phase ϕ (position), frequency ν (velocity), and linear frequency sweep rate α (acceleration) and controlled using a digital sequencer.

Assuming that the AOM frequency is constant (and set equal to the repetition rate of the comb), the beat note of the photodiode will be around 160 MHz. Again, the board is not fast enough to handle such a signal. The demodulation is performed in two steps: first using an analog mixer with a demodulation signal at a frequency close to 160 MHz, and second using an internal I/Q demodulator. The time-dependent frequency demodulation [Eq. (3)] is entirely performed in the analog mixer, and the I/Q demodulator works at a fixed frequency (set at 5 MHz). The output of the I/Q demodulator is fed to a Cartesian to polar converter based on the CORDIC algorithm. The remaining phase, which can be unwrapped around many revolutions, is the measure Φ_{error} of Eq. (4).

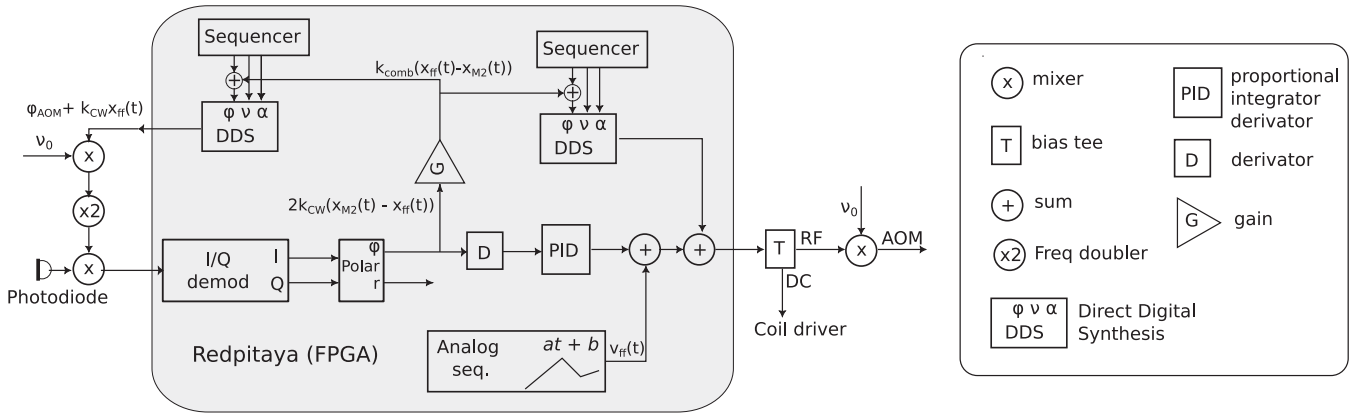

FIG. 2. Schematic of the control system implemented using a red pitaya board. To accommodate for the relatively low bandwidth of the board (50 MHz), we use frequency mixers to shift the frequencies from the digital to analog converter to the AOM and from the photodiodes to the analog to digital converter. The command of the coil driver is digitally added to the rf in the FPGA and then extracted using a bias T to accommodate the limited number of outputs of the board.

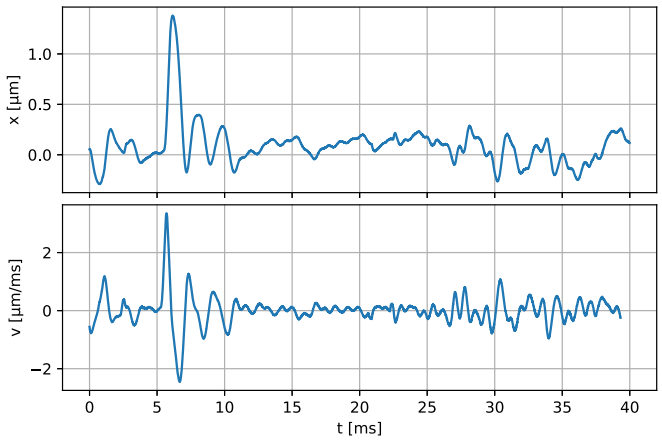

FIG. 3. Performance of the lock on M2 position and velocity. Top: residual error on the position of M2 regarding the atoms' position. The position of M2 can be controlled with an accuracy of up to a few hundred nm. Bottom: residual error on the velocity of M2 regarding the velocity of the atoms. The origin of time corresponds to the release time of the cloud. We observe at $t = 5$ ms an oscillation that corresponds to the change of velocity of the mirror after the first Raman pulse.

The current in the coil is controlled with a voltage, therefore we have to compensate for the electromotive force. This is performed using an analog sequencer that produces linear ramps. On top of this voltage, we apply feedback to control the mirror. Because we control the force, proportional feedback will be unstable. A derivator is used to convert the phase to a signal proportional to the velocity error, which is then fed to a PID and added to the analog sequencer, forming a closed loop.

In Fig. 3 we show the accuracy of the position and the velocity of the translating stage with respect to the command. This scheme allows us to control the position of M2 up to a few hundred nanometers over more than 1 cm.

Yet, as for interferometers driven by cw lasers, controlling the phase difference between the two counterpropagating beams is critical. Because the phase Φ_{atoms} of the atomic cloud depends on $k_{\text{comb}} x_{\text{M2}}(t)$, the residual error in position, shown in Fig. 3, induces a phase noise on the atom of the order of 0.5 rad. To compensate for this phase noise caused by moving mechanical parts, we retroact on the phase of AOM2. We feedback the error in the position shown in Fig. 3 into the phase of the AOM. By doing so, $\Phi_{\text{atoms}} \propto k x_{\text{M2}}(t) + \Phi_{\text{AOM}}(t)$. With the scheme presented in Fig. 2, we are also able to control independently both the position of the mirror and the phase of the laser on the atoms.

In the fixed delay line experiment, for pulses with duration of $\tau \simeq 2$ ps, the size of the overlap region on the order of $c\tau \simeq 600\,\mu$m limits the maximum interrogation time to approximately $\sqrt{2c\tau/g} \simeq 10$ ms. This limitation can also be understood in reciprocal k-space. Indeed, only the average phase $k_{\text{comb}} x(t)$ is compensated using the AOM. There is a remaining dispersion $\Delta_k x(t)$, where $\Delta_k \simeq \frac{1}{c\tau}$ is the dispersion in the wave vector of the pulsed laser. Due to this dispersion, the contrast drops to zero when $\Delta_k x(t) \gtrsim 1$, i.e., $x(t) \gtrsim c\tau$. This also gives a fundamental limit in the precision of the measurement as k_{comb} is not a well-defined quantity. By accelerating the mirror, we maintain the overlap between the laser pulses and the atoms. In doing so, we also compensate for the Doppler shift, each tooth gets the appropriate frequency shift, and the resonance condition is still met. There is no phase dispersion and, consequently, the interrogation time is no longer limited. Furthermore, the sensitivity of our interferometer is limited by the knowledge of the mirror's position, which relies on a precise value of the wave vector k_{CW}. The wave vector of the frequency comb only contributes to a small phase correction applied to the AOM, the average of which is 0.

III. EXPERIMENTAL RESULTS

The experimental setup is described in Ref. [9]. A cloud of cold ^{87}Rb atoms is produced in a magneto-optical trap followed by an optical molasses. The atoms are released by turning off the cooling lasers. During their free fall they are interrogated by a sequence of $\pi/2$ Raman pulses that compose the interferometer. The Raman transitions occur between the hyperfine levels $|5s\ ^2S_{1/2}, F = 1\rangle$ and $|5s\ ^2S_{1/2}, F = 2\rangle$. The laser is detuned by $\Delta/2\pi = 1.1$ THz from the $5s\ ^2S_{1/2} - 5p\ ^2P_{1/2}$ transition, and its waist is 2 mm. The duration of a π Raman pulse is $\tau_\pi \approx 350\,\mu$s, which corresponds to a train of $\tau_\pi f_{\text{rep}} \approx 26\,000$ ps pulses. The optical setup used to control precisely the overlap position of the counterpropagating picosecond pulses is illustrated Fig. 1. To compensate for the Doppler effect induced by the atom's free fall and to satisfy the resonance condition given by Eq. (1), we accelerate the mirror M2 following the procedure detailed in the previous section. The start of this acceleration is synchronized with the release of the atomic cloud.

We have studied two configurations: the first is the usual Ramsey Bordé configuration, consisting of two pairs of $\pi/2$ pulses. The second consists of a sequence of $\pi/2$-π-π-$\pi/2$ pulses where atomic wave packets are interrogated selectively in each arm of the interferometer. This original configuration is not feasible with a cw laser. We detect the fluorescence of atoms in each hyperfine level $|F = 1\rangle$ and $|F = 2\rangle$ using the time-of-flight technique. Atomic fringes are obtained by varying the acceleration α of M2. In this way, we probe the atomic phase at the output of the interferometer: $\Phi \simeq k_{\text{comb}}(g - \alpha)t^2$.

A. Tracking the midpoint trajectory

The displacement of M2 should follow simultaneously the trajectory of the two interfering atomic wave packets over the whole interferometer sequence. A naive solution consists of following their midpoint trajectory. Figure 4 shows the variation of contrast as a function of interrogation time $T = 2T_{\text{R}} + T_{\text{D}}$, where T_{R} is the Ramsey time and T_{D} is the spacing time between the two pairs of $\pi/2$ pulses. The blue point is extracted by fitting the atomic fringe pattern by the cosine's function. The contrast drops by 50% after a total interrogation time of 25 ms. This is a fivefold improvement compared to our previous work, where a 50% drop in contrast was observed for a total duration of 5 ms ($T_{\text{R}} = 2$ ms).

A Monte Carlo simulation is performed to compute the contrast $\mathcal{C}$ of the interferometer. This simulation consists of

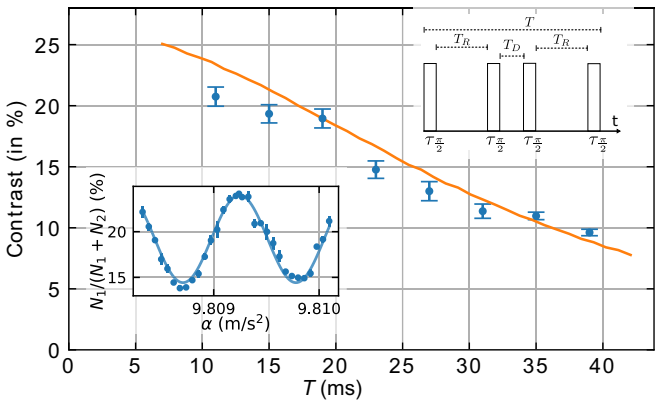

FIG. 4. Contrast of the central fringe as a function of the total interrogation time with $\tau = 1.47$ ps, a π-pulse duration of 0.6 ms, and T_D of 3 ms. Experimental data are shown in blue. The Monte Carlo simulation is shown by the orange full line. Typical fringes are shown in the bottom inset for $T = 39$ ms. The contrast is deduced from a fit of the fringes (blue line). The upper inset shows the interferometer sequence.

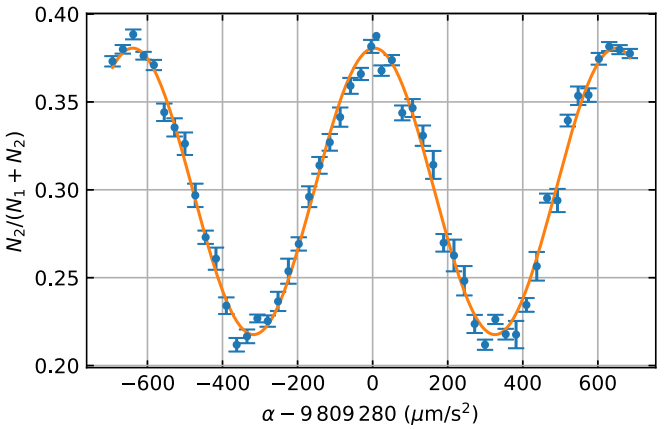

FIG. 6. Atomic fringes at the output of the interferometer: probability to be in the excited state as a function of the acceleration of the mirror M2. Experimental data are shown as blue points. Each point is an average of over five points, with an error bar given by the dispersion of those points. Here $\Delta = 1.1$ THz, $\tau = 1.23$ ps, $T_R = 15$ ms, $T_D = 25$ ms.

applying a pulse sequence $\{\pi/2 - \pi/2\} - \{\pi/2 - \pi/2\}$ to an initial cloud with Gaussian spatial and velocity distributions. Each pulse induces a two-photon Raman transition with a coupling Rabi frequency

$$\Omega(r,z) = \frac{\Omega_0^2}{2\Delta}\mathrm{sech}\left(\frac{z}{c\tau}\right)\exp\left(-\frac{2r^2}{w^2}\right), \tag{5}$$

where Ω_0 and Δ are, respectively, the Rabi frequency and detuning with respect to the one-photon transition, c is the speed of light, τ is the duration of a picosecond pulse, z is the position of the atom with respect to the center of the overlap zone, and r is its transverse position. We then extract the number of atoms a_1 and a_2 in each internal state at one output port of the interferometer. The contrast is given by $\mathcal{C} = 4\langle a_1 a_2\rangle/\langle a_1^2 + a_2^2\rangle$. The experimental data are in good agreement with the simulation (orange line).

This limitation is due to the finite size of the overlap zone. When the two arms of the interferometer are separated by a distance larger than the size of the overlap zone, meaning that the Rabi coupling during the second pulse of the interferometer decreases, the $\pi/2$ criteria are not fulfilled.

B. Interrogating each arm of the interferometer selectively

Raman interaction occurs in the region where the two picosecond pulses overlap. Consequently, when the two interfering wave packets are separated by a distance larger than the spatial extension of a picosecond pulse, it is possible to selectively interrogate one or the other wave packet. This feature allows the use of unusual interferometer configurations. A relevant configuration uses a sequence of pulses $\pi/2$-π-π-$\pi/2$ [16,17]. Figure 5 illustrates two possible schemes, depending on whether the first π pulse catches one or the other wave packet. In the first configuration (Fig. 5, right), the atomic phase difference at the output of the interferometer depends only on external degrees of freedom, whereas in the second configuration (Fig. 5, right), it is sensitive to both external and internal degrees of freedom [16]. In practice, we control the delayed pulse by monitoring the motion of the M2 mirror. The optimal trajectory of this mirror (shown in pink in Fig. 5) ensures that the atoms see the same Rabi frequency at each pulse of the interferometer sequence, which maximizes the contrast of the fringes.

Figure 6 shows typical atomic fringes obtained in the configuration of Fig. 5, left, for a total interrogation time of

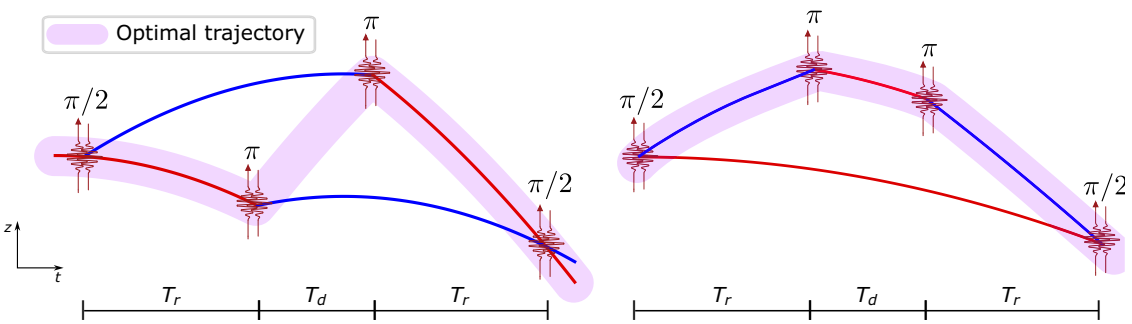

FIG. 5. Illustration of the atomic wave-packet trajectories for a $\pi/2$-π-π-$\pi/2$ pulse sequence. The vertical axis represents the atoms' vertical position, and the horizontal axis is time. The blue and red colors distinguish the internal states. The pink shaded lines show the trajectory of the overlap zone controlled via the M2 mirror.

55 ms and T_R of 15 ms. The interrogation time is limited only by the travel range of the voice coil actuator. The contrast is a fivefold improvement compared with the configuration described in the previous paragraph (two pairs of $\pi/2$ pulses). A fit (continuous orange line) by a cosine function allows us to determine the frequency of the central fringe with a relative uncertainty of 10^{-7}, which corresponds to a sensitivity of about 1 mrad. To test our setup, we performed the same experiment using cw lasers, phase-locked at a fixed frequency. We found that the residual phase noise observed on the atomic fringe was smaller and is therefore not related to the displacement of M2 but comes from the feedback loop on the comb repetition rate. We analyzed the contrast evolution in this configuration using Monte Carlo simulations. The contrast decay is due to two main effects: One is the inhomogeneity of the Rabi coupling (due to the finite length of the picosecond pulses and the transverse size of the laser beam). The second is due to the initial velocity of the atoms as they may escape from the overlap zone.

C. Discussion

It may sound paradoxical to use an atom interferometer based on spatially localized beam splitters to measure the velocity or acceleration of atoms. Simplistic reasoning suggests that the velocity resolution would be given by $\hbar$ divided by the length of the picosecond pulse $c\tau$. For an accelerometer, this would result in a resolution scaling as $\frac{\hbar T_R}{c\tau}$. This is equivalent to stating that the separation of the two arms must not be larger than the picosecond pulses' length. As shown in the previous section, this is not a fundamental limit for the $\pi/2 - \pi - \pi - \pi/2$ interferometer. Indeed, although the Raman interaction is localized, in this scheme we do not know which path the atom took after the first $\pi/2$ pulse, so there is no which-path information.

However, for very long interrogation times, the fact that the Raman coupling is spatially localized will eventually limit the contrast of such an interferometer. Let us consider the ideal case of a plane atomic wave. After a Raman transition, this plane wave transforms into a Gaussian wave packet, with a momentum dispersion of $\Delta p = \frac{\hbar}{c\tau}$. During its evolution, the wave packet spreads out and will no longer overlap perfectly with the interaction zone of length $c\tau$, resulting in a loss of contrast. This limits the duration of the interferometer to $T_{\max} \sim \frac{m(c\tau)^2}{2\hbar}$. In our experimental condition, $T_{\max}$ would be of the order of tens of seconds. If one uses shorter pulses, this effect could be observed. Indeed, using for instance femtosecond pulses, we have $T_{\max} \sim 10$ ms. Note also that the confinement of the initial wave packet increases the energy of the selected wave packet by $(\Delta p^2/2m)$. This change in energy induces a phase shift $\hbar T_R/2m(c\tau)^2$. This phase shift is the analog of the Gouy phase for a Gaussian optical beam. It cancels out in usual calculations where it is assumed that the two interfering wave packets have the same size and therefore undergo the same phase shift [18]. Considering our current experimental parameters, this phase shift is estimated to be 80 μrad, too small to be observed considering the current sensitivity of our interferometer.

IV. CONCLUSION

In this paper, we have presented an atom interferometer with beam splitters that are spatially localized and whose position can be dynamically and precisely controlled during the interferometer sequence. Our robust and flexible setup enables new interferometer configurations while compensating for the Doppler effect. The atomic beam splitters are based on frequency-comb driven Raman transitions, which require pairs of counterpropagating ultrashort pulses to overlap at the atom's position. Our setup allows for accelerating a mirror placed in a delay line to precisely control its position, without introducing noise in the laser phase. We increased the interrogation time by a factor of 5 compared with our previous work, only limited by the travel range of our translation stage. We measured the Earth's gravitational acceleration with a relative statistical uncertainty of around 10^{-7}. A Monte Carlo simulation was carried out to model the effect of the wave-packet separation and showed good agreement with the experimental results. We have implemented an interferometer configuration where the atomic beam splitters interact selectively with the wave packets propagating in either arm of the interferometer, and we have investigated the fundamental limitations of this interferometer.

We have recently carried out a second-order Bragg diffraction and a multi-π atomic beam splitter with a picosecond laser. As the interaction between laser pulses and atoms is localized, laser beams induce two-photon light shifts only on the atoms being interrogated. This is not the case when using a continuous laser, where light shifts inevitably affect both interfering wave packets, leading to spurious phase shifts, loss of contrast, and systematic biases in the measured quantity.

ACKNOWLEDGMENTS

C.S. acknowledges support from Region Ile-de-France through the DIM SIRTEQ Fellowship ELUDA, and from the LabEx ENS-ICFP with the references ANR-10-LABX-0010 and ANR-10-IDEX-0001-02 PSL. This experiment is also supported by the DIM QuanTiP (Quantum Technologies in Paris Region), RYBIA project.

[1] S. Dimopoulos, P. W. Graham, J. M. Hogan, M. A. Kasevich, and S. Rajendran, Phys. Rev. D **78**, 122002 (2008).

[2] P. W. Graham, J. M. Hogan, M. A. Kasevich, and S. Rajendran, Phys. Rev. Lett. **110**, 171102 (2013).

[3] J. M. Hogan and M. A. Kasevich, Phys. Rev. A **94**, 033632 (2016).

[4] R. Geiger, L. Amand, A. Bertoldi, B. Canuel, W. Chaibi, C. Danquigny, I. Dutta, B. Fang, S. Gaffet, J. Gillot, D. Holleville, A. Landragin, M. Merzougui, I. Riou, D. Savoie, and P. Bouyer, in *Proceedings of the 50th Rencontres de Moriond Gravitation* (ARISF, 2015), p. 163.

[5] B. Canuel, S. Abend, P. Amaro-Seoane, F. Badaracco, Q. Beaufils, A. Bertoldi, K. Bongs, P. Bouyer, C. Braxmaier, W.

Chaibi, N. Christensen, F. Fitzek, G. Flouris, N. Gaaloul, S. Gaffet, C. L. Garrido Alzar, R. Geiger, S. Guellati-Khelifa, K. Hammerer, J. Harms *et al.*, Class. Quantum Grav. **37**, 225017 (2020).

[6] A. A. Geraci and A. Derevianko, Phys. Rev. Lett. **117**, 261301 (2016).

[7] A. Arvanitaki, P. W. Graham, J. M. Hogan, S. Rajendran, and K. Van Tilburg, Phys. Rev. D **97**, 075020 (2018).

[8] J. Lee, R. Ding, J. Christensen, R. R. Rosenthal, A. Ison, D. P. Gillund, D. Bossert, K. H. Fuerschbach, W. Kindel, P. S. Finnegan, J. R. Wendt, M. Gehl, A. Kodigala, H. McGuinness, C. A. Walker, S. A. Kemme, A. Lentine, G. Biedermann, and P. D. D. Schwindt, Nat. Commun. **13**, 5131 (2022).

[9] C. Solaro, C. Debavelaere, P. Cladé, and S. Guellati-Khelifa, Phys. Rev. Lett. **129**, 173204 (2022).

[10] J. N. Eckstein, A. I. Ferguson, and T. W. Hänsch, Phys. Rev. Lett. **40**, 847 (1978).

[11] A. Marian, M. C. Stowe, J. R. Lawall, D. Felinto, and J. Ye, Science **306**, 2063 (2004).

[12] N. Picqué and T. W. Hänsch, Nat. Photon. **13**, 146 (2019).

[13] R. K. Altmann, L. S. Dreissen, E. J. Salumbides, W. Ubachs, and K. S. E. Eikema, Phys. Rev. Lett. **120**, 043204 (2018).

[14] L. S. Dreissen, C. Roth, E. L. Gründeman, J. J. Krauth, M. G. J. Favier, and K. S. E. Eikema, Phys. Rev. A **101**, 052509 (2020).

[15] A. Grinin, A. Matveev, D. C. Yost, L. Maisenbacher, V. Wirthl, R. Pohl, T. W. Hänsch, and T. Udem, Science **370**, 1061 (2020).

[16] Ch. J. Bordé, Phys. Lett. A **140**, 10 (1989).

[17] M. Zimmermann, M. A. Efremov, A. Roura, W. P. Schleich, S. A. DeSavage, J. P. Davis, A. Srinivasan, F. A. Narducci, S. A. Werner, and E. M. Rasel, Appl. Phys. B **123**, 102 (2017).

[18] P. Storey and C. Cohen-Tannoudji, J. Phys. II France **4**, 1999 (1994).